

Microscopic Production Characteristics of Pore Crude Oil and Influencing Factors during Enhanced Oil Recovery by Air Injection in Shale Oil Reservoirs

Meng Du,* Zhengming Yang,* Chun Feng, Lanlan Yao, Xinliang Chen, and Haibo Li



Cite This: *ACS Omega* 2023, 8, 18186–18201



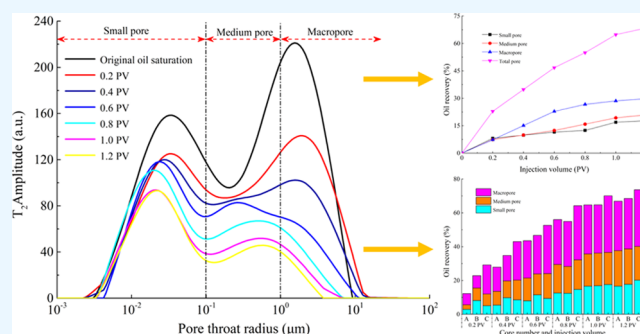
Read Online

ACCESS |

Metrics & More

Article Recommendations

ABSTRACT: High-pressure air injection (HPAI) is one of the effective methods to improve shale oil recovery after the primary depletion process. However, the seepage mechanisms and microscopic production characteristics between air and crude oil are complicated in porous media during the air flooding process. In this paper, an online nuclear magnetic resonance (NMR) dynamic physical simulation method for enhanced oil recovery (EOR) by air injection in shale oil was established by combining high-temperature and high-pressure physical simulation systems with NMR. The microscopic production characteristics of air flooding were investigated by quantifying fluid saturation, recovery, and residual oil distribution in different sizes of pores, and the air displacement mechanism of shale oil was discussed. On this basis, the effects of air oxygen concentration, permeability, injection pressure, and fracture on recovery were studied, and the migration mode of crude oil in fractures was explored. The results show that the shale oil is mainly found in $<0.1 \mu\text{m}$ (small pores), followed by $0.1\text{--}1 \mu\text{m}$ (medium pores), and $1\text{--}10 \mu\text{m}$ (macropores); thus, it is critical to enhancing oil recovery in pores less than 0.1 and $0.1\text{--}1 \mu\text{m}$. The low-temperature oxidation (LTO) reaction can occur by injecting air into depleted shale reservoirs, which has a certain effect on oil expansion, viscosity reduction, and thermal mixing phases, thereby greatly improving shale oil recovery. There is a positive relationship between air oxygen concentration and oil recovery; the recoveries of small pores and macropores can increase by 3.53 and 4.28%, respectively, and they contribute 45.87–53.68% of the produced oil. High permeability means good pore-throat connectivity and greater oil recovery, and the production degree of crude oil in three types of pores can be increased by 10.36–24.69%. Appropriate injection pressure is beneficial to increasing the oil–gas contact time and delaying gas breakthrough, but high injection pressure will result in early gas channeling, which causes the crude oil in small pores to be difficult to produce. Notably, the matrix can supply oil to fractures due to the mass exchange between matrix fractures and the increase of the oil drainage area, and the recoveries of medium pores and macropores in fractured cores increased by 9.01 and 18.39%, respectively; fractures can act as bridges for matrix crude oil migration, which means that proper fracturing before gas injection can make the EOR better. This study provides a new idea and a theoretical basis for improving shale oil recovery and clarifies the microscopic production characteristics of shale reservoirs.



1. INTRODUCTION

As a promising area in global unconventional oil exploration and development, shale oil has received attention as an economic resource due to its great reserve potential.^{1–3} Shale oil usually refers to the oil resources produced by enrichment in organic-rich shale formations.^{4,5} By the end of 2021, shale oil production in North America accounted for more than 50%, reaching 4.67×10^8 t, and the successful exploration and development of shale oil in North America have contributed to the development of the shale oil theory in China. China contains extremely abundant shale oil resources, which are widely distributed in the Ordos Basin, the Junggar Basin, and the Bohai Bay Basin, and the technically recoverable resources could reach $(30\text{--}60) \times 10^8$ t; thus, shale oil has become an important alternative resource in

China's major oilfields for increasing reserves and production.^{6,7} At present, shale oil is mainly based on the depletion development of horizontal wells and volume fracturing. However, since shale reservoirs are characterized by considerable nanoscale pores, the poor pore-throat connectivity, crude oil occurrence characteristics, and production mechanism of shale reservoirs are different from those of conventional

Received: March 8, 2023

Accepted: April 26, 2023

Published: May 10, 2023



reservoirs, all of which make the effective development of shale oil difficult with three major issues: rapid production decline, difficult energy supplement, and poor development efficiency.^{8–11} Additionally, limited by the rapid depletion of crude oil in natural fractures and the slow replenishment of matrix crude oil, it is difficult for shale reservoirs to achieve sustainable exploitation. Therefore, it is urgent to explore advanced development methods because large amounts of crude oil in the matrix have not been effectively produced.

Previous studies have demonstrated that gas injection (natural gas, CO₂, N₂, and air) can effectively improve the development of shale oil.^{12,13,26} In comparison, natural gas, CO₂, and N₂ have the disadvantages of gas shortage and high cost, but air/oxygen-reducing air flooding has attracted much attention due to its obvious advantages of the wide gas source, low cost, and various reservoir types.^{13,14,25} On the other hand, the LTO reaction of air/oxygen-reducing air with crude oil also plays an important role in enhanced oil recovery (EOR). Currently, extensive efforts have been made to study oil oxidation characteristics and EOR mechanisms of air/oxygen-reducing air flooding.^{18,26} Qian et al.¹⁵ studied the mechanism and oxidation characteristics of EOR under different injection pressures via core air flooding experiments. Kok et al.¹⁶ investigated the thermodynamic characteristics of different crude oils using thermogravimetrics and microcommercial thermogravimetrics and concluded that lighter oils are more susceptible to LTO reactions. Liao et al.¹⁷ analyzed the applicable type of air flooding and the characteristics of oxidation dynamics in the whole temperature domain and proposed that the critical oxygen content of air flooding is 10%. Ren et al.¹⁸ studied the LTO process of crude oil in cores and established a model of the LTO reaction. Wang et al.¹⁹ studied the effects of temperature, pressure, and reaction time on the LTO of crude oil through static oxidation tube experiments and analyzed the regulation of air flooding on the physical properties of crude oil from oxygen consumption and produced gas–liquid composition. In general, most studies have focused on the LTO characteristics of light crude oil during gas flooding.^{17,20,26} However, the LTO characteristics of air flooding in shale oil reservoirs are not fully understood.

In recent years, the mechanism of EOR by air flooding has remained a major concern in the development of shale oil, especially the production characteristics of pore throats with different sizes in shale reservoirs under different influencing factors.^{21–23,34} Therefore, based on the oxidation characteristics of crude oil, some scholars have studied the mechanism of air injection to EOR in shale oil by the physical simulation method. Youwei et al.²⁴ believed that the mechanism of air flooding EOR of shale oil is mainly due to the formation of N₂ flooding after crude oil consumes oxygen. N₂ can maintain the reservoir pressure, and the heat and CO₂ generated by LTO can reduce the viscosity of crude oil and expand its volume. Chen et al.²⁵ applied a two-dimensional visualization model to carry out oxygen-reducing air flooding experiments and analyzed the characteristics of oil and gas migration. Qi et al.²⁶ employed cyclotron resonance mass spectrometry and gas chromatography to compare the composition changes of crude oil after LTO and investigated the degree of production of crude oil via oxygen-reducing air flooding. Li et al.²⁷ discussed the influence of gas injection pressure, permeability, fracture, and other factors on the development effect through gas flooding experiments. The above studies mostly used conventional displacement equipment or a static oxidation tube. However, the shale

reservoirs are characterized by a tight lithology, small pore throats, and high capillary pressure, and as a result, conventional experimental research has a large measurement error, which is greatly affected by experimental conditions and human operation. Therefore, some scholars have studied the production mechanism of shale oil based on numerical simulation and microfluidic systems. Yu et al.²⁸ reported the influence mechanism of fracture morphology and injection pressure on the shale reservoir development effect through numerical simulation. Nguyen et al.²⁹ studied the mechanism of EOR by gas injection and quantified the recovery of crude oil in a fracture network via the microfluidic system. Also, some scholars have adopted numerical simulation methods to study the influence mechanism of the injection rate, fracture, oil production rate, and other factors on gas flooding recovery.^{30–32} Furthermore, NMR has been considered to be a key method for the realistic evaluation of fluid flow in porous media. Wan et al.³³ found that injecting gas into shale reservoirs to enhance oil recovery can not only produce large pore crude oil but also recover remaining oil within 0.1 μm small pores. The production degree of small pores is related to the physical properties of shale reservoirs. Huang et al.³⁴ suggested the effects of gas injection pressure, soaking time, and fractures on the production characteristics of crude oil in shale pores from the microscopic scale by NMR. Zhu et al.³⁵ concluded the recovery mechanism and influencing factors of bound oil and movable oil in shale reservoirs based on NMR. Compared with CT, NMR plays a crucial role in determining the core pore size distribution, fluid content, and residual oil distribution. In summary, most current research has focused on oxidation dynamic characteristics, shale oil recovery, and the optimization of injection parameters. However, few scholars have considered the mechanism and influencing factors of air flooding from the microscopic pore production regularity, residual oil saturation, and swept area; in particular, there is a lack of visualization and quantitative research on the characteristics of pore crude oil production and displacement development mechanism in the process of air flooding.

In this study, using a high-temperature and high-pressure physical simulation experiment system, supplemented by NMR online testing technology, an online NMR dynamic physical simulation method for shale oil air injection EOR was established in response to these issues. The injection process in microscopic pores, oil recovery, and residual oil saturation in different pores during air injection of shale oil were investigated via real-time monitoring of pore oil saturation distribution and the oil production process. The micropore production characteristics of different sizes were analyzed, and the oil recovery mechanism of shale oil air flooding was discussed. Based on this, the effects of air oxygen content, permeability, gas injection pressure, and fractures on the shale air flooding effect and pore crude oil production were considered. To the best of our knowledge, the research method proposed in this study is the first to combine the online NMR, microscopic pore production of the reservoir, and air injection for shale oil reservoirs. The novelty of this paper is that the microscopic production characteristics of air flooding in shale oil reservoirs are evaluated from the pore scale and it provides a new method and ideas for the efficient development of shale oil.

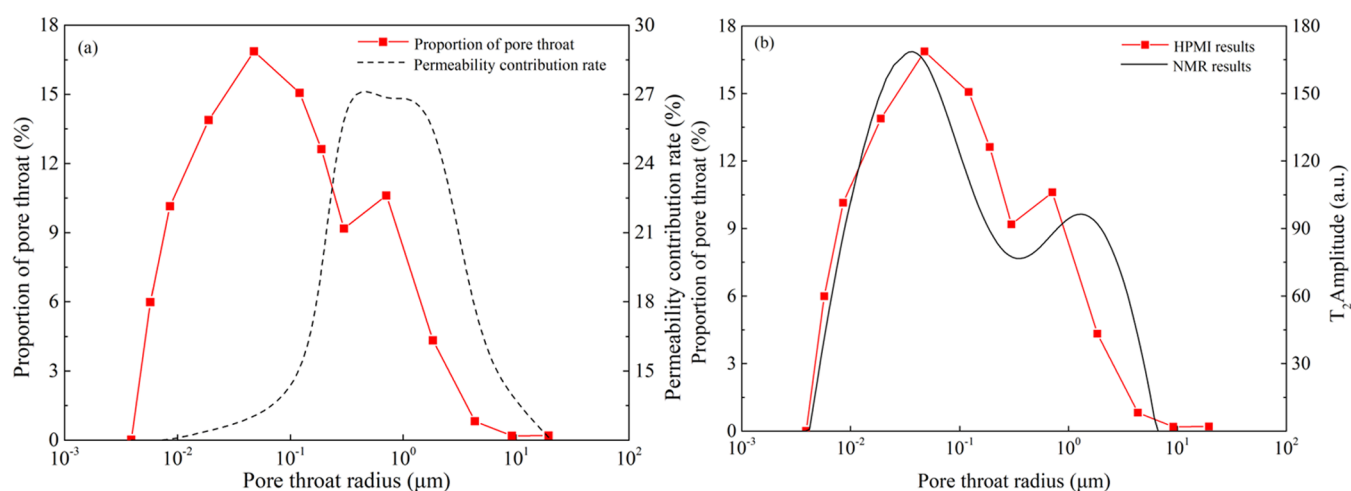


Figure 1. Pore-throat distribution of shale samples (a) and NMR pore size conversion results (b).

2. ONLINE NMR DYNAMIC PHYSICAL SIMULATION EXPERIMENT

When using a conventional experimental device to carry out gas flooding experiments, the fluid production process inside the core is a black box, and as a result, there are some issues in quantitatively analyzing the fluid saturation distribution and migration mechanism inside a core. An online air flooding experimental platform was established by NMR, and crude oil distributed in pores of different scales can produce signals during NMR tests. By real-time monitoring the dynamic migration characteristics of pore crude oil and the amplitude change of the T_2 spectrum signal, the quantitative effect of pore crude oil production and the residual position of residual oil in different pores during air flooding can be obtained. Thus, the microscopic oil displacement mechanism and influencing factors of air injection to EOR in shale oil can be clarified. Moreover, through the online physical simulation experiment of air flooding, the core was placed in the holder during the experiment, that is, the whole experiment was carried out under the condition of a completely closed core, and the test error of stress and core position change can be avoided when the core is taken out.

2.1. Experimental Principle. Based on the low-field NMR theory, nuclear magnetic resonance occurs when hydrogenated protons are immersed in a static magnetic field and exposed to a second oscillating magnetic field. Under the same NMR parameters, the signal intensity is positively correlated with the number of hydrogen protons of hydrogen-containing crude oil in the core. It has been proved that the attenuation curve related to pore size is a single exponential function, and the attenuation coefficient is positively correlated with pore size.^{10,36}

The fluid inside the large pores is less affected by the molecular surface force, the attenuation relaxation speed is slow, and the T_2 value is large. Conversely, the small pores are subjected to a larger molecular surface force, and the T_2 value is small. Moreover, it has been proved that the pore-throat distribution obtained by high-pressure mercury injection (HPMI) has a good correlation with NMR; thus, in this study, the relationship between the NMR conversion coefficient and the relaxation time T_2 spectrum was calibrated based on the HPMI experimental results of shale samples.

First, HPMI experiments were carried out by cutting parallel samples with a length of ~ 2.5 cm from the experimental samples. Figure 1a shows the proportions of the pore-throat distribution

and the permeability contributions of the sample obtained from the capillary pressure curves. It can be seen that the pore-throat distribution shows a typical bimodal distribution, which can be divided into 3 orders of magnitude. The pore-throat radii of the sample are mainly within 0.01–10 μm, and the main pore throats contributing to seepage are 0.35–1.85 μm. Although the distribution of the proportion of small-scale pore throats is much higher than that of the large-scale pore throats, the permeability of the tight shale oil reservoir is mainly contributed by the large-scale pore throats. Moreover, the NMR test was carried out on cores saturated with crude oil; thus, the T_2 spectrum could be obtained using the iterative reconstruction technique (SIRT algorithm). The expression for the T_2 relaxation time can be written as follows^{37,38}

$$M(t) = \sum_i A_i \exp\left(-\frac{t}{T_{2i}}\right) \quad (1)$$

$$\frac{1}{T_2} = \frac{1}{T_{2B}} + \frac{1}{T_{2S}} + \frac{1}{T_{2D}} \quad (2)$$

where T_2 is the relaxation time (ms); T_{2B} and T_{2S} are the transverse relaxation times of the filling fluid and the rock particle surface (ms), respectively; and T_{2D} is the transverse relaxation time caused by fluid diffusion in magnetic field gradients (ms).

In practical experiments, T_{2B} and T_{2D} are often negligible,^{34,38} that is, the T_2 relaxation time can also be expressed as

$$\frac{1}{T_2} = \rho \left(\frac{S}{V} \right)_{\text{pore}} = F_s \left(\frac{\rho}{r} \right) \quad (3)$$

Thus, the relationship between the aperture r and the transverse relaxation time T_2 is as follows

$$r = \rho \times F_s \times T_2 \quad (4)$$

$$r = C \times T_2 \quad (5)$$

where ρ is the surface relaxation strength (μm/ms), S is the pore surface area (cm²), V is the pore volume (cm³), F_s is the pore geometry factor (spherical pore, $F_s = 3$; columnar pore, $F_s = 2$; fissure, $F_s = 1$), r is the pore size (cm), and C is the NMR conversion coefficient.

Based on the pore size conversion results, it can be seen that the HPMI experiment results have a high correlation with the

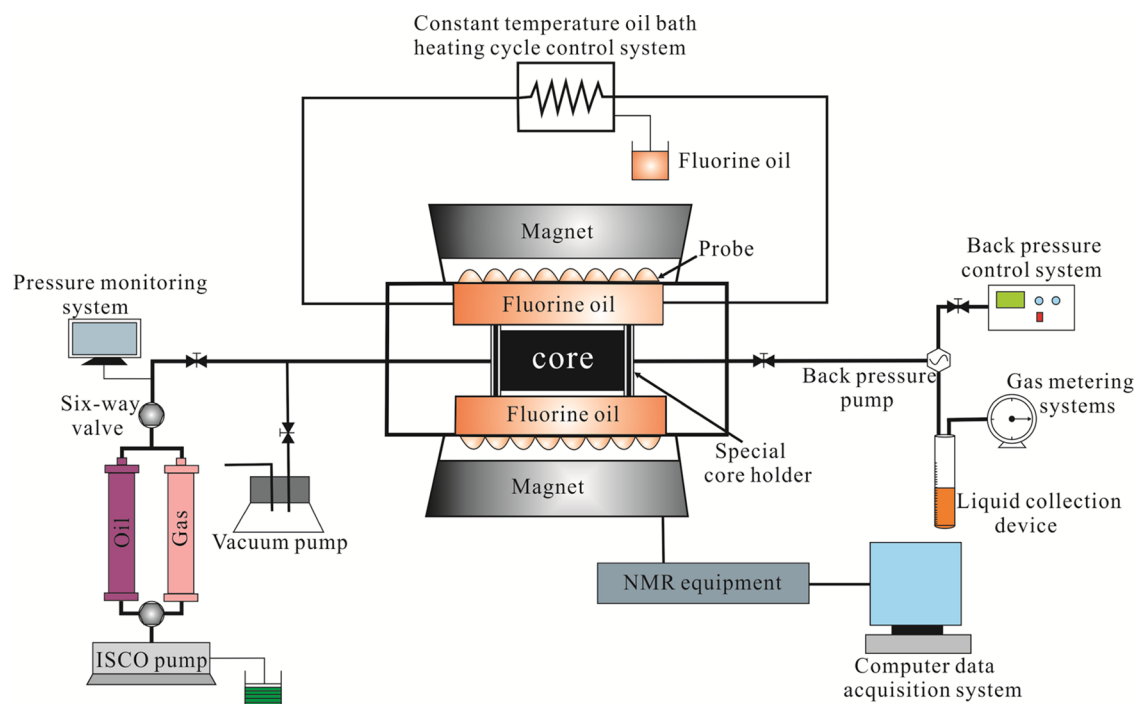


Figure 2. Online NMR dynamic physical simulation experimental system diagram of air injection in shale oil reservoirs.

Table 1. Physical Parameters of Core Samples Using an Online NMR Dynamic Physical Simulation Experiment

no.	diameter (cm)	length (cm)	porosity (%)	permeability ($10^{-3} \mu\text{m}^2$)	injection schemes	influencing factors
A	2.492	6.913	15.1	0.301	(3% O ₂) air	effect of oxygen concentration
B	2.491	7.015	14.8	0.299	(10% O ₂) air	
C	2.501	6.917	14.9	0.302	(21% O ₂) air	
D	2.508	6.829	9.7	0.201	(21% O ₂) air	effect of core permeability
E	2.499	6.726	15.7	0.657	(21% O ₂) air	
F	2.501	6.937	14.6	0.131	28 MPa injection pressure; (21% O ₂) air	effect of injection pressure
G	2.503	6.892	14.2	0.130	34 MPa injection pressure; (21% O ₂) air	
H	2.498	6.943	14.9	0.129	38 MPa injection pressure; (21% O ₂) air	
I	2.504	6.918	13.5	0.121	matrix-type; (21% O ₂) air	effect of fractures
J	2.498	6.935	17.2	0.563	fractured-type; (21% O ₂) air	

pore size converted according to the NMR T_2 spectrum (Figure 1b). Moreover, according to the change of the NMR T_2 spectrum area, oil recovery can be calculated by

$$G = \frac{S_1 - S_2}{S_1} \quad (6)$$

where G is the oil recovery (%) and S_1 and S_2 are the integration of the T_2 spectrum in saturated oil and after flooding, respectively.

2.2. Experimental Apparatus and Materials. The NMR online air flooding experimental system of shale oil reservoirs was developed by combining a high-temperature and high-pressure displacement physical simulation device and NMR technology (Figure 2). The system mainly consisted of three parts: (a) a constant-temperature oil bath heating cycle control system: the experimental temperature confining pressure was controlled by circulating fluorine oil around the core holder, and the experimental temperature and pressure could reach 90 °C and 50 MPa, respectively; (b) a displacement physics simulation system, which consisted of a displacement pump, a special core holder, a back-pressure control system, and a liquid collection device; and (c) an NMR experimental system: the model was

MacroMR12, the resonance frequency was 12.798 MHz, and the magnet strength was 0.3 T. The shortest echo time of the device was 0.1 ms, which could capture the fluid signals of the nanoscale pore throats in the tight rock samples. The parameter settings during the NMR experiment had a great influence on the results, and the test coefficients needed to be determined according to the core. Generally, the NMR test had four test coefficients: the echo interval (TE), scan number, waiting time (RD), and echo number (NECH). If the NECH is large, the accuracy of the equipment can be improved, but the test time will significantly increase. Similarly, if the RD is too short, the macropore signal will be lost, but if the RD is too long, the test time will be significantly prolonged. Therefore, before each experiment, the parameters of the nuclear magnetic T_2 spectrum were adjusted first, and central frequency calibration, electronic shimming, and hard pulse amplitude adjustment were carried out according to the sample conditions.

The experimental cores were collected from the shale reservoirs of the Permian Lucaogou Formation in Jimsar Sag, Junggar Basin. The 10 shale samples from this area were selected to carry out porosity and permeability tests; the porosity was measured using a porosimeter (PORG-200), the permeability was measured using the helium method, and the depths of the

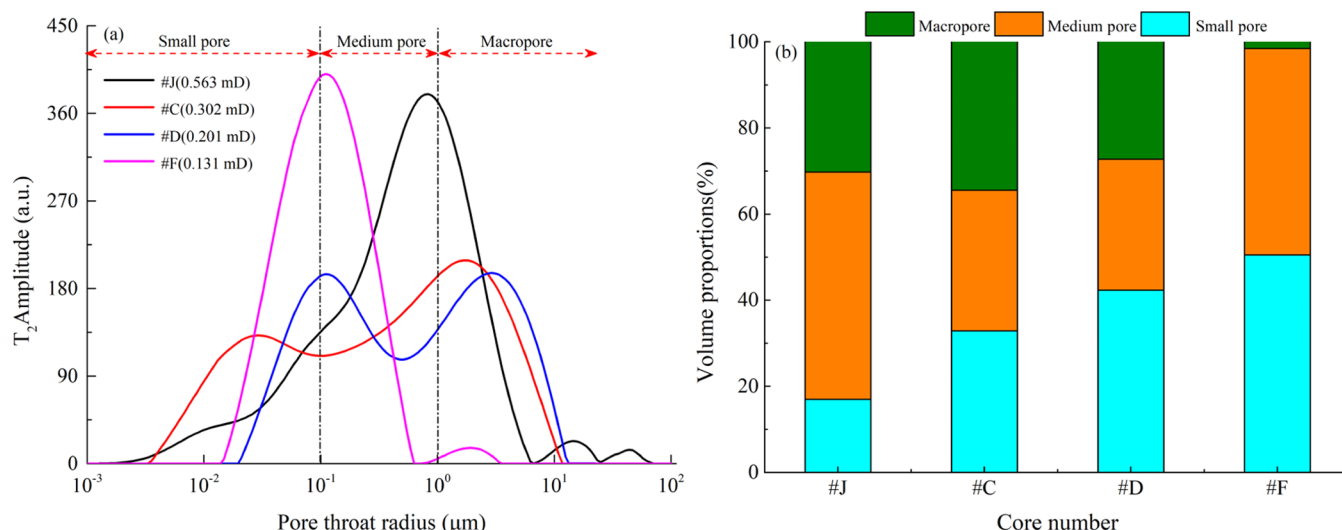


Figure 3. NMR T_2 spectrum distribution of samples after saturated oil (a) and the pore distribution of samples converted from the NMR T_2 spectrum (b).

core samples were 3490–3630 m. The porosity and permeability of the samples were 9.7–17.2% and $(0.121 - 0.657) \times 10^{-3} \mu\text{m}^2$, respectively. The diameter of the samples was ~ 2.50 cm, the lengths were 6.0–7.0 cm, and they were collected parallel to each other in the longitudinal direction. The basic physical parameters of the core are shown in Table 1. The gases employed in the experiment were oxygen-reducing air (3% oxygen concentration), oxygen-reducing air (10% oxygen concentration), and high-pressure compressed air (21% oxygen concentration). The oil used in the experiment was crude oil from the study area. Its viscosity was 10.41 mPa·s under formation conditions (85 °C), and its density was 0.886 g cm^{-3} .

2.3. Experimental Procedure.

- (1) The oil and salt in the core were washed out, and the core was dried for 24 h. The raw T_2 spectral curve of the sample was obtained.
- (2) The experimental temperature was gradually increased to 85 °C, and the core was evacuated, saturated with crude oil, and aged. The T_2 spectra of the crude oil-saturated samples were tested, and the relationship between the oil volume and NMR semaphore was constructed via NMR calibration. The saturated oil volume and porosity were calculated using the gravimetric method and the NMR method.
- (3) The gas was injected into the sample by a high-pressure displacement pump, and the experimental conditions remained unchanged. NMR tests were conducted at different injection volumes (0.2, 0.4, 0.6, 0.8, 1.0, 1.2 PV), and the gas and oil samples were collected at the outlet for chromatographic analysis. When the spectral line no longer changed, the experiment was terminated, and the oil saturation changes of the pores were calculated according to the changes in the spectral lines.
- (4) Steps (1)–(3) were repeated on different oxygen concentration (3% O_2 , 10% O_2 , 21% O_2) air, different permeability samples (0.201×10^{-3} , $0.657 \times 10^{-3} \mu\text{m}^2$), and different types of samples (matrix type, fractured type).
- (5) Steps (1) and (2) were repeated. Under different injection pressures (28, 34, 38 MPa), the NMR tests were conducted at different displacement times (2, 4, 6, 8,

10, 12 h), and the NMR signal correction with a standard sample ensures that the experimental results are comparable during the scanning test.

3. EXPERIMENTAL RESULTS AND DISCUSSION

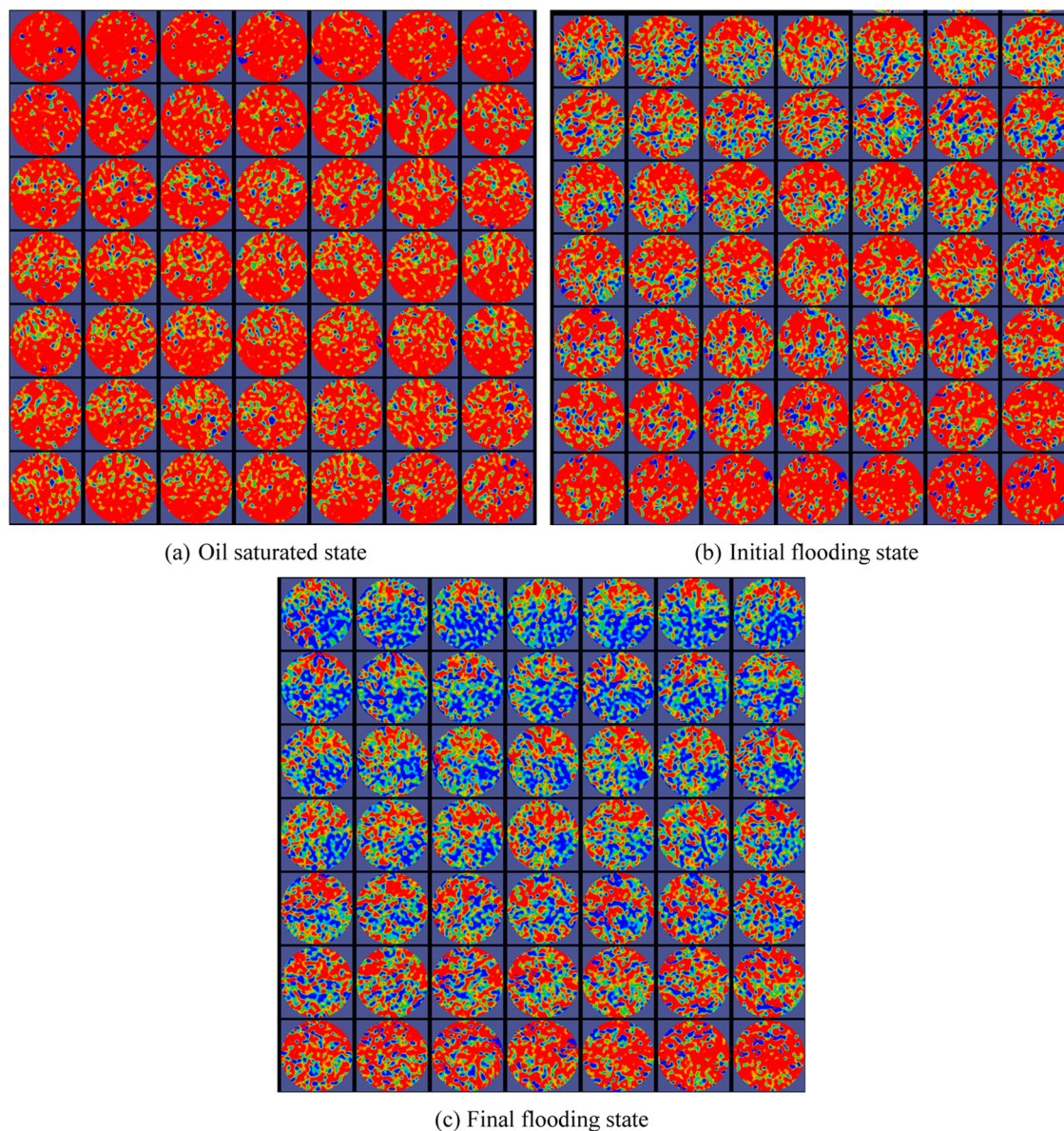
3.1. Pore Structure Characterization and Oil Saturation of Shale Core.

The NMR T_2 spectra of shale samples after oil saturation are shown in Figure 3a, and the pore distributions of the samples converted from the NMR T_2 spectra are shown in Figure 3b. The shape, range, and width of the T_2 spectra distributions can illustrate the pore size distribution characteristics and pore connectivity. In general, the macropores correspond to a longer relaxation time and the smaller pores correspond to a shorter relaxation time. It can be seen that the T_2 spectrum exhibits a relatively obvious bimodal distribution with a high right peak and a low left peak. The pores can be divided into small pores ($< 0.1 \mu\text{m}$), medium pores ($0.1 - 1 \mu\text{m}$), and macropores ($1 - 10 \mu\text{m}$), and the corresponding T_2 relaxation times are < 5 , 5–50, and 50–500 ms, respectively (Table 2). Overall, the average pore radius of more than 75% of

Table 2. Pore Classification and NMR T_2 Value Correspondence Table

pore type	NMR T_2 value range (ms)	pore size range (μm)
small pores	< 5	< 0.1
medium pores	5–50	0.1–1
macropores	50–500	1–10

the shale samples in this area is less than $1 \mu\text{m}$. When the core permeability is $(0.131 - 0.201) \times 10^{-3} \mu\text{m}^2$, the proportion of smaller pores is more than 42%, with the increase of core permeability, the proportion of medium pores and macropores increases gradually. When the core permeability is $0.563 \times 10^{-3} \mu\text{m}^2$, the proportion of medium pores and macropores is about 83%, indicating that the pore structure of the rock is closely related to the permeability. With increasing permeability, the distribution range of the T_2 widens, and the main peak shifts to the medium pores and macropores. This is relatively consistent with the HPMI results: the lower the core permeability, the larger the proportion of nanopores. It can be concluded that



(a) Oil saturated state

(b) Initial flooding state

(c) Final flooding state

Figure 4. Two-phase saturation changes of shale samples C in different states of air flooding.

there was deterioration of physical properties and pore-throat connectivity, reduced average pore radius, and decreased pore sorting with decreasing permeability.

The online NMR spectrometer is applied to record the NMR T_2 data of saturated crude oil samples, and the hydrogen signal value is a direct reflection of crude oil.³⁹ The formula for calculating the initial oil saturation P_{oci} is

$$P_{\text{oci}} = \frac{\sum_{T_{2,\min}}^{T_{2,\max}} A_{i,j} - \sum_{T_{2,\min}}^{T_{2,\max}} A_{i,b}}{\sum_{T_{2,\min}}^{T_{2,\max}} A_{i,o} - \sum_{T_{2,\min}}^{T_{2,\max}} A_{i,b}} \times 100\% \quad (7)$$

where P_{oci} is the oil content (%); $T_{2,\min}$ and $T_{2,\max}$ are the minimum and maximum T_2 relaxation times, respectively (ms); and $A_{i,j}$, $A_{i,o}$, and $A_{i,b}$ are the corresponding signal strength values of NMR T_2 relaxation time curves of saturated oil, the signal strength of oil-bearing NMR after different core experiments, and the NMR spectrometer base semaphore, respectively (A m^{-1}).

According to the T_2 spectrum of saturated oil (Figure 3b), the oil is mainly distributed in the pores of 0.005–10 μm , the crude oil content in the medium pores and macropores was about 65%, and the proportion of small-pore crude oil decreases with the decrease of permeability. The reasons for this phenomenon can be summarized as follows. (1) Small pores are mainly nanopores and micro-nanopores with a radius of less than 100 nm. Although the proportion of these pores is large, it is difficult for crude oil molecules to enter them under the normal displacement pressure gradient. Moreover, it is generally considered that the oil mobility in nanopores is low, and the core pore connectivity will deteriorate with the increase of the proportion of small pores. (2) The complex minerals of shale reservoirs are randomly distributed, resulting in uneven wettability of the rock surface, that is, the water-wet area shows a reticular distribution and the oil-wet area shows a dispersed distribution, which belongs to mixed wetting.^{27,34} In particular, small pores are usually oil-wet, and oil cannot enter them via imbibition due to insufficient capillary force. Therefore, it is more difficult to saturate crude oil with decreasing core permeability.

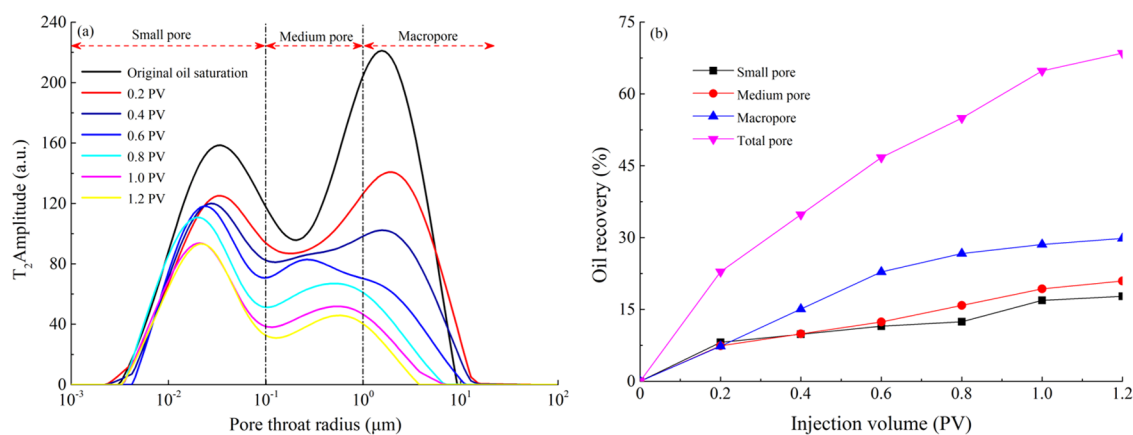


Figure 5. Air flooding NMR T_2 spectra of shale samples (a) and the relationship between the pore recovery degree with different sizes and injection volume (b).

3.2. Microscopic Pore Crude Oil Production Characteristics of Shale Samples by Air Flooding. The CT scanning imaging was performed on the oil-saturated state, the initial flooding state, and the final flooding state of shale sample C, and the air swept area and residual oil distribution were investigated to realize the visual comparison of air swept pore throats (Figure 4). The red areas correspond to the crude oil, and the blue areas correspond to the injected air. Meanwhile, based on the NMR theories and the air flooding T_2 spectrum of shale samples at different injection volumes, the microscopic production characteristics of crude oil in different scale pores were quantitatively evaluated, and the air flooding T_2 spectrum of shale sample C is shown in Figure 5a. Combined with Figures 4 and 5a, it can be seen that the crude oil saturation is sufficient in the initial state (Figure 4a). With the increase of air injection volume, the color of the model changes from red to blue, indicating that the gas phase enters the inlet of the model from the left to the right. The oil saturation at the 1/3 plunger of the inlet end is decreased (Figure 4b), and the T_2 spectrum shows a downward trend (Figure 5a), indicating that the crude oil with different scales of pores in shale samples can be effectively produced under air flooding.

Furthermore, as shown in Figure 5a, the envelope of the left peak as well as the right peak decreases significantly at 0.2 pore volume (PV) air injection. This demonstrates that the oil saturation of small pores, medium pores, and macropores is decreased. On increasing the air injection volume to 0.4 PV, the apex of the right peak moves downward, and the apex of the left peak decreases slightly, indicating that the oil production from macropores is increasing. On further increasing the air injection volume to 0.8 PV, the right envelope moves to the left, the width of the T_2 spectrum narrows, and the apex of both the left and right peaks moves down, indicating that both medium-pore and macropore oil are produced significantly. On increasing the air injection volume to 1.0 PV, the apex of the left peak exhibits a decreasing trend, indicating that the oil production of small pores such as nanopores is increased. On the continuous increase of the air injection volume to 1.2 PV, the amplitude change of the envelope curve becomes weak, indicating that the lower limit of movable oil is reached. It can be obtained that air flooding development mainly produces crude oil with pores sizes of 0.01–10.00 μm , and the oil in the pore sizes of 6–10 μm is completely displaced. The core outlet is the main enrichment area of residual oil, and the residual oil is mainly distributed in the small pores and the medium pores (Figures 4c and 5a). Also,

the chromatographic analysis of the produced oil sample found that the heavy components such as asphaltene increased, indicating that the LTO reaction occurred between oil and oxygen during air displacement. Overall, in the early stage, the area of the spectral peaks decreased rapidly, while the spectral peaks changed slowly in the later stage, indicating that the oil production degree was high in the early stage, and the production rate continued to decrease in the later stage.

Figure 5b shows the relationship between the pore production degree and the air injection according to the T_2 spectrum, and there are obvious differences in the production characteristics of the pores with different scales. The oil in the macropores was preferentially produced under a small air injection volume, the growth rate of the production degree increased first and then decreased, and the production degree reached more than 29%. The production degree of medium pores gradually increases with the increase of air injection, almost showing a linear increase trend, but the growth rate gradually decreases in the later stage. The production degree of the small pores slowly increased, and the overall production degree was small, reaching 17–20%. It is noteworthy that the recovery degree of small pores shows an obvious inflection point when the air injection volume is 1.0 PV, and the production degree increases significantly, which is in good accordance with the NMR T_2 spectrum.

It can be concluded that the macropores had less flow resistance, which was more conducive to gas flow and had a greater degree of production. However, the connectivity of small pores was poor, so the production degree was small. Additionally, further analysis suggested that this was also related to the swept position of air in the core pores and the pathway of the fluid migration. The high-pressure air first swept the macropores with a small seepage resistance; meanwhile, the oil was enriched and circulated in the macropores and was displaced by the high-pressure air, which greatly increased the production from the macropores. In the later stage, the pressure was gradually transmitted to the small nanoscale pores. Under the action of the pressure difference and the LTO reaction, the oil in the small nanoscale pores flowed into the macropores and migrated to the outside through the macropores. Therefore, it can be summarized from the above results that the production rate of the macropores oil was initially fast and then slow, exhibiting a higher degree of utilization, while the production of the oil of the small and medium pores exhibited a slowly increasing trend, and the overall production degree was lower. Also, the low production from the small pores can also be attributed to the

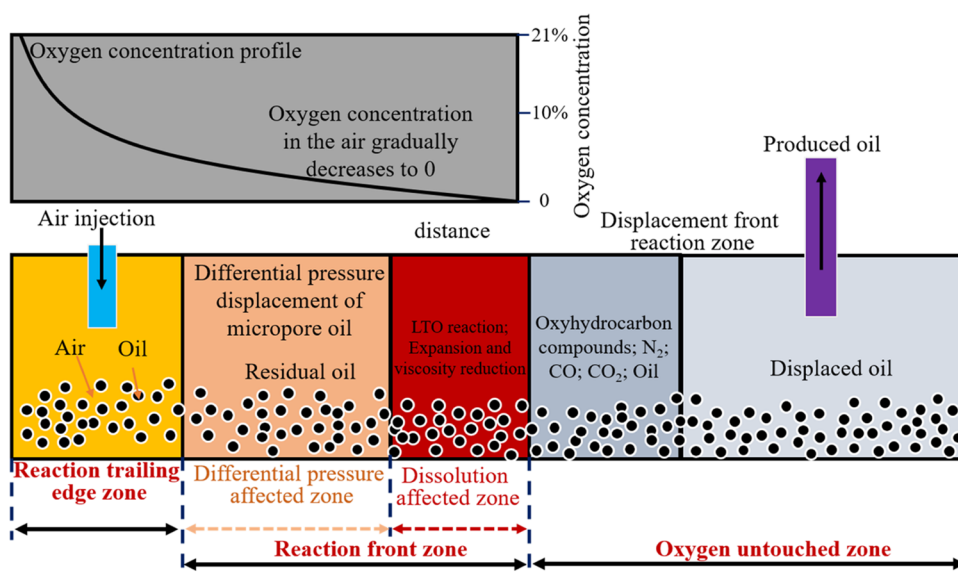


Figure 6. Shale reservoir air flooding EOR displacement mechanism diagram.

binding effect between the nanopores and the fluid molecules, which is called the nanoconfinement effect.³⁹ The correlation analysis results are in good accordance with those of previous studies.^{34,39}

3.3. Air Flooding Mechanism of Shale Oil Reservoir.

Based on the difference between the air flooding sweep mode and pore oil production characteristics, the air flooding process can be divided into the reaction trailing edge area, the reaction front area, and the oxygen-untouched area (Figure 6). Among them, the reaction front area can be divided into pressure difference sweep and dissolution sweep. The main oil flooding mechanism of the pressure difference sweep is that high-pressure air enters the matrix pores under the action of differential pressure, and the oil in the matrix pores is displaced by the pressure difference. The main oil recovery mechanism of dissolution sweep is the LTO reaction when oxygen is in sufficient contact with oil, that is (1) hydrocarbon compounds such as CO, CO₂, ether, aldehyde, and ketone produced by the LTO reaction can expand the volume of pore crude oil, reduce viscosity, and enhance fluidity; (2) the mass exchange between oil and gas makes air and LTO reaction products further dissolve into microporous oil, which can effectively supplement the formation energy; and (3) with the decrease of formation pressure, the gas dissolved in crude oil can be separated to form dissolved gas flooding, and N₂ flooding can also be formed due to the consumption of oxygen in the air. In addition, the light components extracted from oil, CO, and CO₂ can also play the role of flue gas flooding, that is, flue gas continuously extracts low carbon components from oil, which continuously enriches the injected gas and makes its properties close to those properties of oil; the slow component mass transfer of crude oil occurs under the action of extraction, which continuously depletes the oil and makes its properties close to those properties of injected gas. Thus, the oil–gas interfacial tension will decrease, and gas and oil can form miscible flooding or partially thermal miscible flooding at high pressure and high temperature.^{34,40} As a result, an air flooding high-temperature front reaction zone can be formed under various oil flooding mechanisms, which corresponded to the bulldozing effect proposed by Gutierrez et al.⁴⁰ This high-temperature reaction front zone will push the formation oil forward, like a bulldozer, which can greatly

increase the oil recovery. In addition, Xi et al.⁴¹ proposed that air flooding can form a thermal miscible reaction front, and the oil displacement mechanism can be composed of flue gas flooding, N₂ flooding, and the LTO reaction. Meanwhile, the LTO reaction can accelerate the advance of the thermal miscible front and the carbon bond stripping effect, and the air fire flooding can be formed under the accumulation of reaction heat; the generated thermal effective pressure can also play a role in miscible flooding, gasification/distillation, expansion and viscosity reduction, thereby increasing shale oil recovery through thermal flooding and miscible flooding.

It is worth noting that the injection timing of air flooding in shale oil reservoirs is extremely important. When the depletion pressure is low, the reservoir energy cannot be supplemented in time. The rapid decrease of pressure in pores and fractures will cause a sharp increase of effective stress, resulting in stress sensitivity of gas injection and a significant decrease of oil recovery. This can be attributed to the fact that although the micropores and fractures in the core matrix are widely developed, the complex storage and migration spaces such as the intragranular dissolved pores and cement micropores in the core were not strongly compacted during the formation process, and as a result, the micron-scale mineral particles are loosely cemented and gas-sensitive clay minerals are distributed in the pores. It can be deduced that under the action of air flooding, these mineral particles would dissolve or slip, and the contact relationship and arrangement of the mineral particles would change, easily blocking the nano-micron-scale pore throats.^{39,42} Therefore, this gas sensitivity phenomenon will reduce the core permeability and result in poor air injection effect, and the argillaceous cemented minerals in the core mainly exhibit plastic deformation, which is difficult to effectively recover.

4. INFLUENCING FACTORS OF AIR FLOODING EOR

According to the T_2 spectrum, the total oil recovery and different scale pore recovery can be calculated. This study focuses on the effects of oxygen concentration, permeability, injection pressure, and fractures on pore oil production during air flooding. The influencing factors of EOR by air injection in shale oil reservoirs are illustrated by the microscopic pore scale, and the relevant calculation results are shown in Table 3.

Table 3. Online NMR Dynamic Physical Simulation Experiment Results of Air Flooding under Different Influencing Factors

no.	influencing factors	permeability ($10^{-3} \mu\text{m}^2$)	total oil recovery (%)	proportion of crude oil recovery in different scales of pores (%)		
				small pores	medium pores	macropores
A	oxygen concentration	0.301	66.88	16.62	21.01	29.25
B		0.299	68.49	17.74	20.92	29.83
C		0.302	73.68	20.15	20.01	33.53
D	permeability	0.201	29.50	1.34	11.23	16.93
E		0.657	77.44	26.03	24.12	27.29
F		0.131	28.60	12.64	17.01	-1.05
G	injection pressure	0.130	54.81	22.48	27.35	4.98
H		0.129	39.45	27.82	8.17	3.46
I		0.121	34.55	14.89	10.88	8.78
J	fractures	0.563	58.03	10.97	19.89	27.17

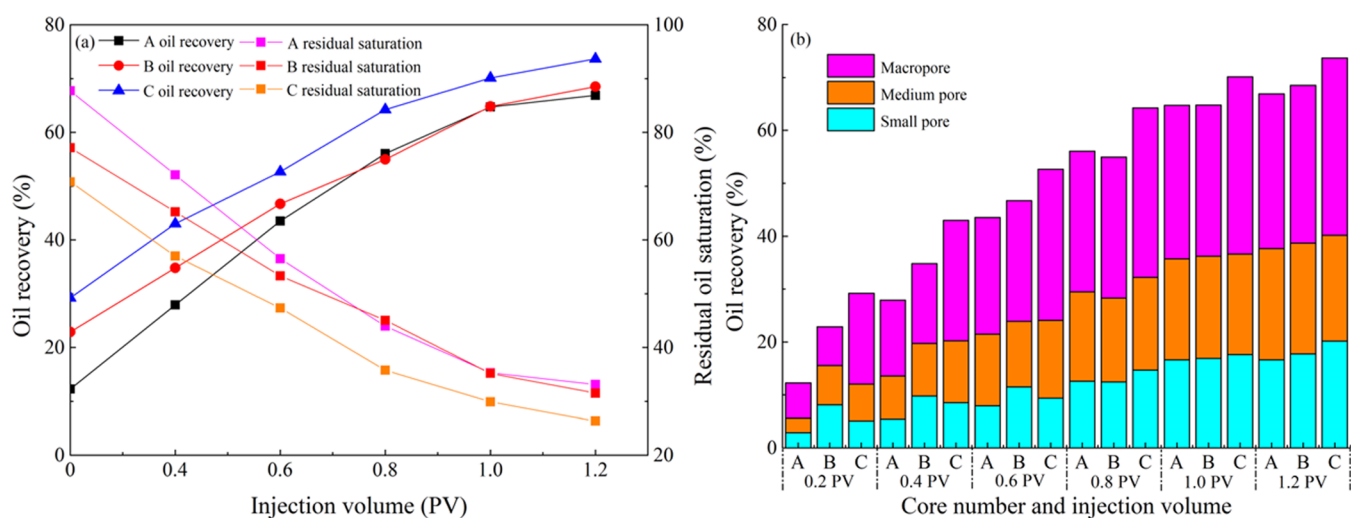
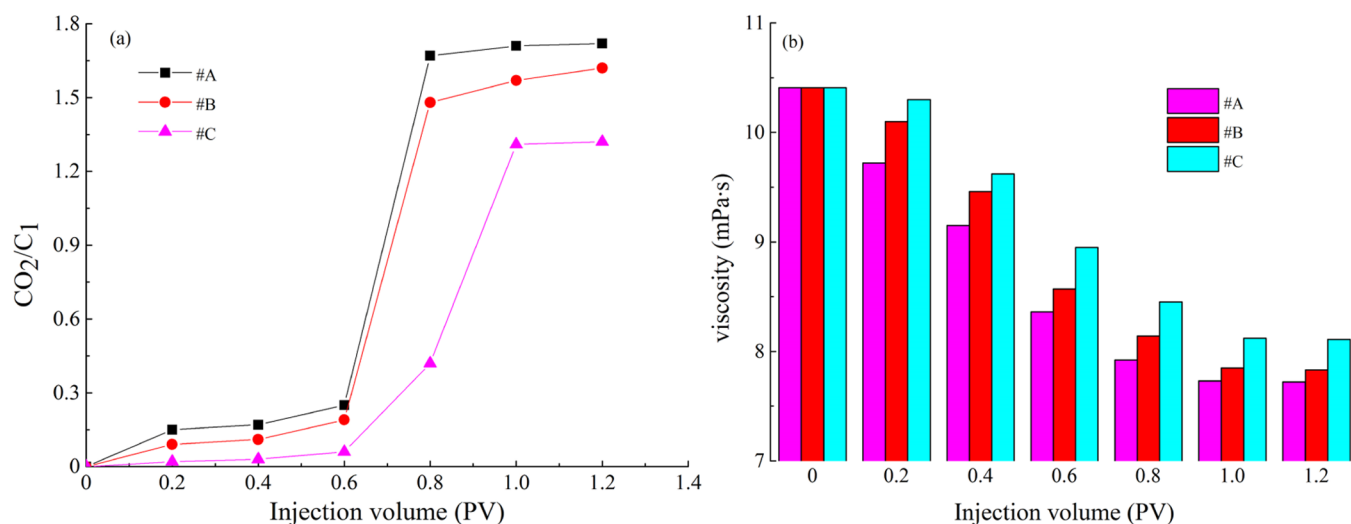


Figure 7. Change of total oil recovery (a) and different pore recoveries (b) as a function of injection volume of air flooding with different oxygen concentrations in shale samples.

Figure 8. Change of the CO_2/C_1 value (a) and crude oil viscosity (b) as a function of injection volume of air flooding with different oxygen concentrations.

4.1. Effect of Oxygen Concentration. The change of oil recovery with injection volume under different oxygen concentration air floodings is shown in Figure 7a. The oil recovery increases rapidly with the air injection volume before the air injection volume is 0.8 PV. When the air injection volume

is 0.8 PV, in oxygen-reducing air (3% O_2) flooding, the recoveries for small pores, medium pores, and macropores are all lower. In oxygen-reducing air (10% O_2) flooding, the recoveries for small pores, medium pores, and macropores are 3.16, 5.65, and 4.49%, respectively. However, in air (21% O_2) flooding, the

recoveries for small pores, medium pores, and macropores can be increased by 2.24, 1.68, and 5.36%, respectively. When the air injection volume is 1 PV, the recovery degree slows down, indicating that the injected air gradually reaches the upper limit of pore-throat production. Overall, the oil recovery of the three samples presents a trend of increasing rapidly and then decreasing slowly. As the air oxygen concentration increased from 3 to 21%, the oil recovery increased from 66.88 to 73.68%, with an increase of 6.80% and a nearly linear increase trend. Meanwhile, compared with the production degree of different pores (Figure 7b), the recovery of small pores increased from 16.62 to 20.15%, and the recovery of macropores increased from 29.25 to 33.53%, with increases of 3.53 and 4.28%, respectively. The recovery of medium-pore oil remained at about 21.65%. It is noteworthy that the oil recovery of small pores and macropores increases with the increase of oxygen concentration, and they contribute 45.87–53.68% of the produced oil, indicating that the increase of air oxygen concentration is favorable to the improvement of oil production.

From the above results, it can be concluded that when the oxygen concentration is low (3%), the gas composition is mainly N_2 , and the injected gas mainly plays a similar role as N_2 flooding. That is, the N_2 gas molecule is small and can preferentially enter the medium-pore and macropore oil of the core to supplement the formation energy. Also, when the reservoir pressure decreases, the gas dissolved in the oil can be released, and dissolved gas flooding can occur under the effect of pressure difference, all of which make the medium-pore and macropore oil recovery higher.³³ Yet, N_2 has a poor production on small-pore oil because it is almost insoluble in oil.

Since the ratio of CO_2 to C_1 in the oil is a fixed value, the CO_2/C_1 value in the produced gas is defined as the amount of CO_2 generated in the LTO reaction and the degree of the LTO reaction. Figure 8a shows that the CO_2/C_1 value increases with injection volume, and the higher the oxygen concentration, the higher the CO_2/C_1 value. It can be observed that when the oxygen concentration is high (21%), the LTO reaction can occur when the oxygen in the air repeatedly contacts the oil, and the degree of LTO reaction increases with the oxygen concentration. Moreover, the formed hydrocarbon compounds such as CO_2 and aldehydes by the LTO reaction can act as the surfactant, which can reduce the interfacial tension and viscosity of small-pore crude oil (Figure 8b). Meanwhile, the LTO reaction promotes mass transfer between crude oil and air, which makes the resin asphalt generated by the LTO reaction block the dominant channel in the core, thereby reducing the gas channeling phenomenon and increasing the swept area. Furthermore, from the above analysis of the air flooding mechanism, with the decrease of crude oil viscosity, the light components in oil and flue gas can form a supercritical thermal miscible front zone under the action of thermal expansion, and the resulting thermal miscible flooding and flue gas flooding can greatly improve the recovery of small-pore oil, thereby increasing the total oil recovery.^{26,40} It is worth noting that during high-oxygen-concentration air flooding, the stronger LTO reaction makes the temperature of the core holder slightly increase, which proves that the LTO reaction can increase the reservoir temperature. Limited by the short contact time of oil and gas under experimental conditions, the oxidation effect is not sufficient. As a result, in the actual field, the oxygen concentration of air flooding can be increased within a safe range, and the EOR will be better.

Figure 9 exhibits the residual oil saturation of shale samples under air flooding with different oxygen concentrations. As the

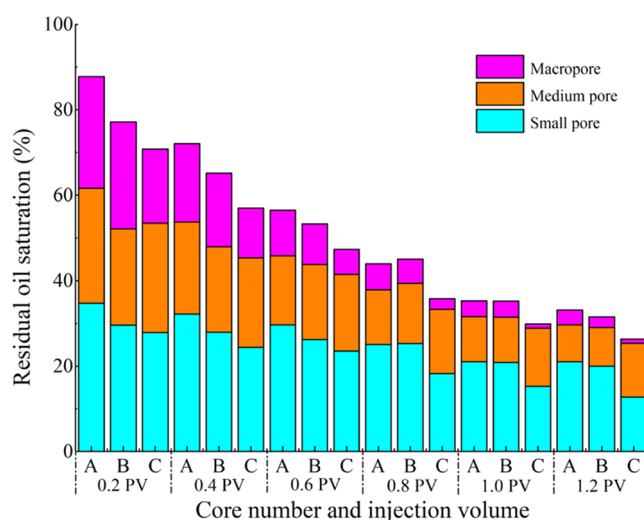


Figure 9. Change of residual oil saturation as a function of injection volume of air flooding with different oxygen concentrations.

air oxygen concentration increased from 3 to 21%, the residual oil saturation after air flooding decreased from 33.12 to 26.32%. The residual oil saturation of small pores reached 21.00, 19.99, and 12.27%, respectively; the residual oil saturation of medium pores reached 21.00, 19.99, and 12.27%, respectively; and the residual oil saturation of macropores reached 3.48, 2.50, and 0.97%, respectively. In general, at the same permeability level, compared with low-oxygen-concentration air flooding, the residual oil saturation after high-oxygen-concentration air flooding is 5.18–6.81% lower. Especially in small pores, the residual oil saturation after high-oxygen-concentration (21%) air flooding is less than that of low-oxygen-concentration (5%) air flooding by 8.23%. The residual oil is mainly distributed in medium and small pores of less than $1 \mu\text{m}$, and in macropores, residual oil is less. This further indicates that under the same injection volume, high-oxygen-concentration air flooding is more conducive to the recovery of small-pore and macropore crude oil.

4.2. Effect of Core Permeability. Figure 10a presents the change of oil recovery under air flooding with different permeability samples. The oil recovery in the low-permeability sample ($0.201 \times 10^{-3} \mu\text{m}^2$) shows a trend of slow and then rapid increase, while the oil recovery in the high-permeability sample ($0.657 \times 10^{-3} \mu\text{m}^2$) exhibits a trend of increasing rapidly and then slowly; the increase in the high-permeability sample is consistently higher. When the air injection volume was 0.8 PV, the recoveries for small pores, medium pores, and macropores in high-permeability samples reached 21.53, 21.96, and 25.78%, respectively; compared with the low-permeability samples, the recoveries of medium-pore and macropore oil increased by 14.43 and 10.76%, respectively. Overall, the total oil recovery increased from 29.50 to 77.44% with the permeability increasing from 0.201×10^{-3} to $0.657 \times 10^{-3} \mu\text{m}^2$. Also, the recovery of small pores increased from 1.34 to 26.03%, the recovery of medium pores increased from 11.23 to 24.12%, and the recovery of macropores increased from 16.93 to 27.29%, with increases of 24.69, 12.89, and 10.36%, respectively (Figure 10b). Results indicated that high permeability means better pore-throat connectivity and strong fluid flow ability. Some air entering

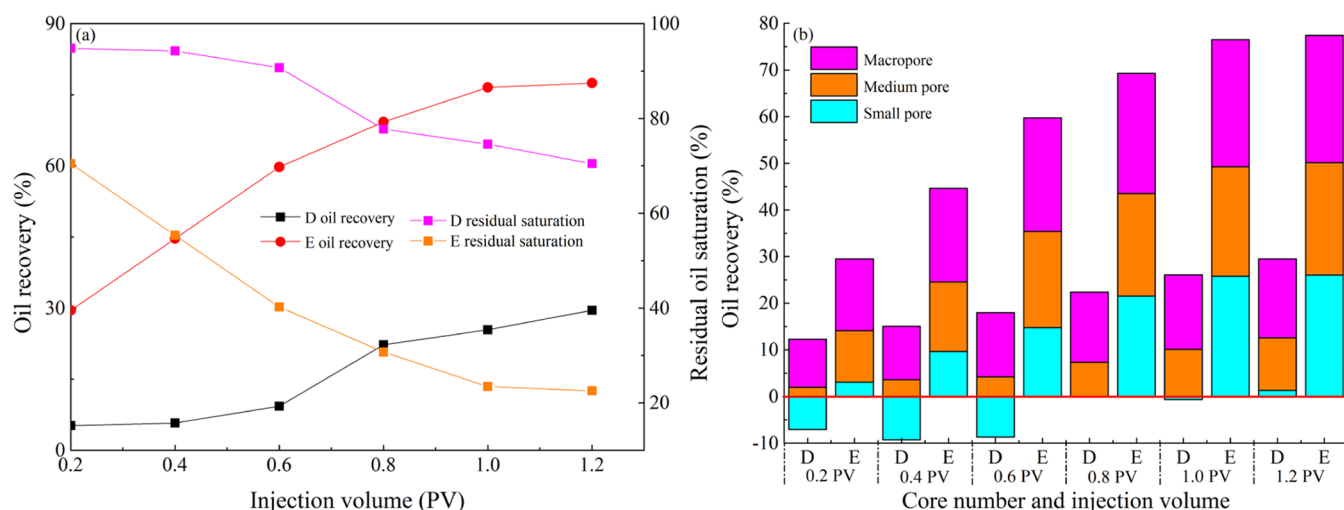


Figure 10. Change of total oil recovery (a) and different pore recoveries (b) as a function of injection volume of air flooding with different permeability samples.

the macropores can successfully overcome the capillary pressure and flow to the smaller pores around, and as a result, not only macropore crude oil can be effectively produced but also nanoscale small pores can be produced to a higher degree, and oil is more easily produced.

It should be pointed out that the small-pore T_2 spectrum of low-permeability samples increases slightly and then decreases during air flooding, which is reflected in Figure 10b that the recovery of small-pore oil decreases below zero and then increases above zero. It can be deduced that the negative oil recovery is due to the air-carrying part of the crude oil transferred to smaller pores during air flooding, which redistributes the residual oil. In the later stage, the injected air is an excess phase relative to the crude oil, and the air can contact the small-pore oil to lead to the LTO reaction, resulting in the change of the physical properties of the crude oil and its discharge.

The residual oil saturation of shale samples with different permeabilities under air flooding is shown in Figure 11. As the permeability increased from 0.201×10^{-3} to $0.657 \times 10^{-3} \mu\text{m}^2$, the residual oil saturation after air flooding decreased from 70.49

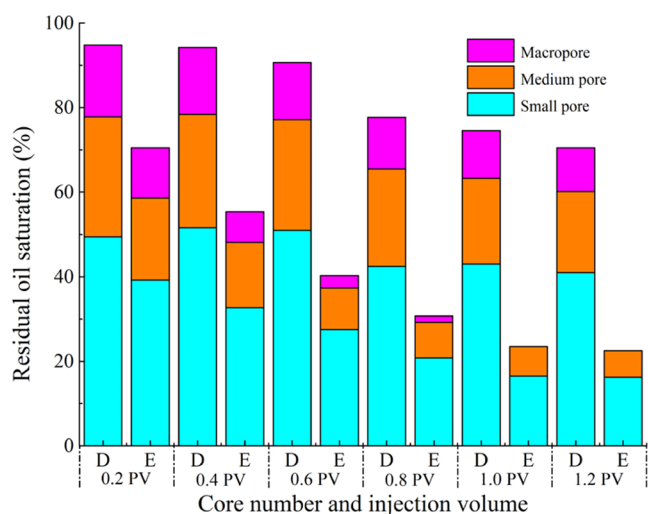


Figure 11. Change of residual oil saturation as a function of injection volume of air flooding with different permeability samples.

to 22.56%. The residual oil saturation of small pores reached 40.97 and 16.15%, respectively; the residual oil saturation of medium pores reached 16.16 and 6.28%, respectively; and the residual oil saturation of macropores reached 10.36% and zero, respectively. Overall, at the same air injection volume, compared with the low-permeability sample, the residual oil saturation after the high-permeability-sample air flooding was 47.93% lower. Especially in small pores and macropores, the residual oil saturation values of high-permeability-sample air flooding were 24.82 and 10.36% lower than those of low-permeability samples, respectively. It can be concluded that the low-permeability samples have strong heterogeneity during gas flooding, and the gas first spreads to the relatively high-permeability area, which makes the oil saturation in the relatively high-permeability area decrease obviously; in the relatively low-permeability area, there is a bypass effect due to poor pore connectivity, so the degree of oil production is low.^{9,25} Therefore, in the actual field, the shale reservoir should be fractured to improve the reservoir seepage capacity before air injection development, which will greatly improve the shale oil recovery.

4.3. Effect of Injection Pressure. The injection pressure mainly affects the microscopic pore sweep area of the core by affecting the stability of the oil and gas front. Al-Mudhafar et al.⁴³ reported that the injection pressure has a significant influence on the displacement front and recovery, that is, when the displacement pressure is less than the critical pressure, stable displacement with high recovery can be obtained. Figure 12a presents the change of oil recovery with injection volume under different injection pressure air floodings. When the air injection time was 10 h, at 34 MPa air flooding, the recovery values for small pores, medium pores, and macropores reached 22.22, 26.73, and 4.92%, respectively; the small-pore and medium-pore oil recovery values were 10.69 and 9.03% higher than that at 28 MPa air flooding, respectively. Overall, as the air injection pressure increased from 28 to 38 MPa, the oil recovery values were 28.60, 54.81, and 39.45%, respectively, showing a trend of increasing first and then decreasing. Also, the recovery of small pores increased from 12.64 to 27.82%, and the recovery of medium pores increased from 17.01 to 27.35% and then decreased to 8.17%. The recovery values of macropores are -1.05, 4.98, and 3.46%, respectively (Figure 12b). It can be observed that the recovery degree of macropore oil is negative

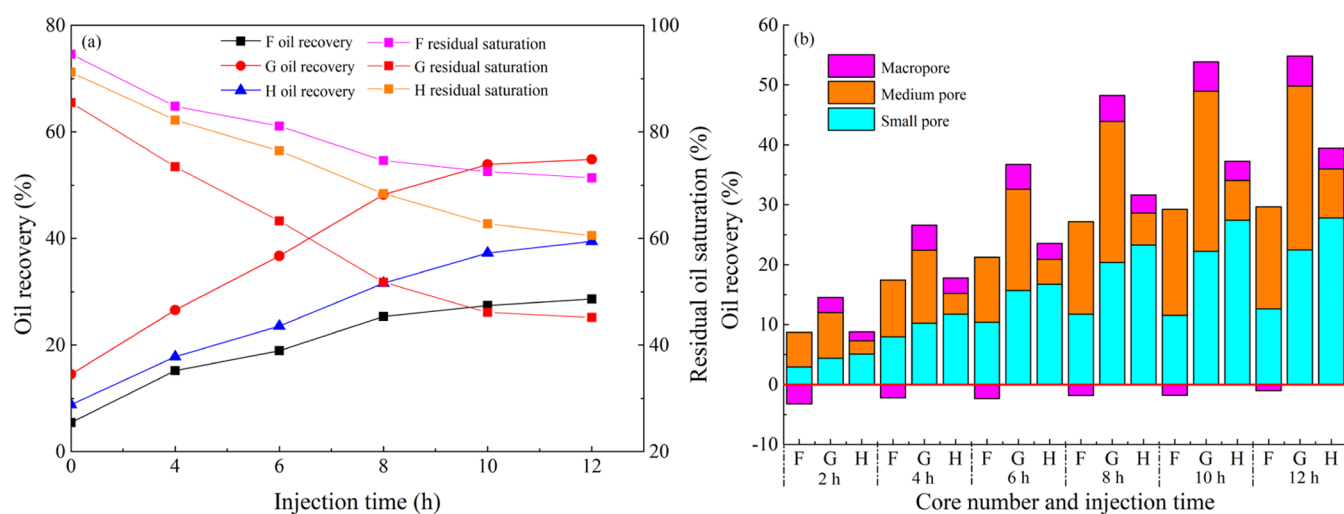


Figure 12. Change of total oil recovery (a) and different pore recoveries (b) as a function of injection volume of air flooding with different injection pressures.

under 28 MPa injection pressure displacement, indicating that the air-carrying part of the oil transferred to macropores during air flooding, which makes the residual oil redistributed. Thus, macropores can play a role in oil discharge.

The experimental results suggest that under appropriate displacement pressure, air can slowly diffuse to nanoscale small pores, and small-pore oil can sufficiently contact with air. When the internal action energy of air is close to the activation energy of small-pore oil, according to the similar solubility, the solubility of air in crude oil is improved and the total oil recovery is increased. Also, increasing the injection pressure can increase the gas diffusion and component mass transfer rate, that is, air can enter some small pores under high injection pressure, thereby increasing the degree of oil production. However, the total amount of air entering the small pores is limited due to the fine pore throat and the slow pressure conduction. Thus, the effect of dissolved gas flooding in the later stage is weak, and even the larger injection pressure has little effect on the recovery of small-pore oil. Meanwhile, high-pressure air will gather inside the core to form a continuous gas-phase zone, and the gas viscosity will increase. When the viscous force is greater than the pore capillary force, the fingering phenomenon will occur, resulting in easier gas channeling; as a result, the contact area and contact time of oil and gas decrease, which makes some small pores of the sample difficult to be affected, and most of the residual oil remains in the dead-end pores. This explains that the recovery of medium-pore and macropore oil decreases under high injection pressure, resulting in the lowest oil recovery. Therefore, the actual field gas injection pressure parameters should be optimized to avoid excessive gas injection pressure, leading to gas channeling to production wells, which will hinder safe production.

The residual oil saturation of shale samples under different injection pressure air floodings is shown in Figure 13. As the air injection pressure increased from 28 to 38 MPa, the residual oil saturation reached 71.40, 45.19, and 60.55%, respectively. The residual oil saturation of small pores reached 37.83, 12.87, and 57.38%, respectively; the residual oil saturation of medium pores reached 30.94, 29.53, and 3.16%, respectively; and the residual oil saturation of macropores reached 2.26, 2.79%, and zero, respectively. Overall, at the same permeability level, compared with 28 and 38 MPa air flooding, the residual oil saturation after

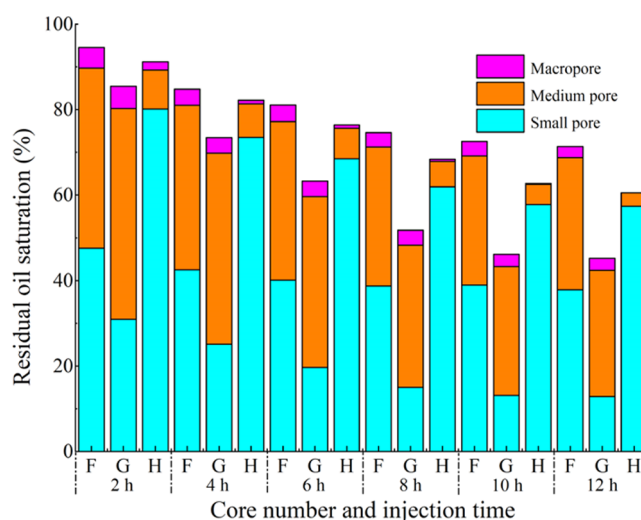


Figure 13. Change of residual oil saturation as a function of injection volume of air flooding with different injection pressures.

34 MPa air flooding is 10.85–26.21% lower, and especially in small pores, the residual oil saturation is 10.85–26.21% lower.

4.4. Effect of Fracture. Fractures are the key to shale oil enrichment and production. Combined with field logging and digital core data, it can be observed that shale reservoirs develop a variety of microfractures such as small-angle interlayer bedding fractures, structural fractures, diagenetic shrinkage fractures, and plane slip fractures, which are arranged in layers of light and dark interaction.^{44,45} The horizontal layer connectivity is better than the vertical connectivity. This indicates that fractures can improve the effectiveness of reservoirs and increase the seepage capacity of shales, which provides a necessary migration channel for shale oil to enter the well from matrix pores. That is, fractures have a great impact on the development of shale oil–gas injection.

Figure 14 exhibits the T_2 spectrum of the fractured-type sample under different air injection volumes. It can be seen that the fractured-type sample not only distributes small pores, medium pores, and macropores but also has two T_2 peak signals in the pore size greater than 11 μm . The signal amplitude decreases with the increase of air injection volume, which is

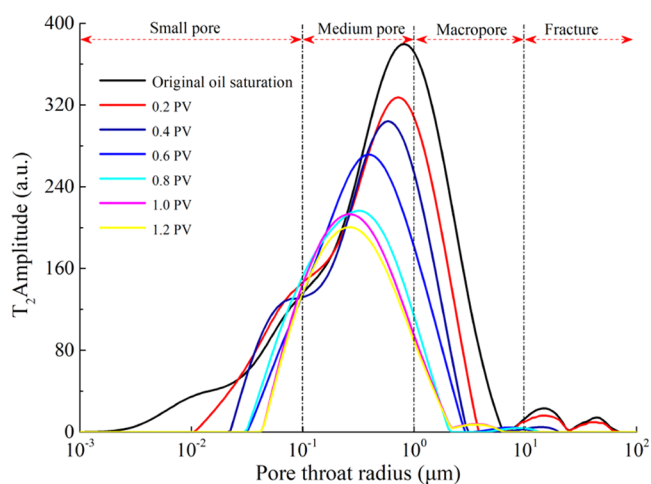


Figure 14. Air flooding NMR T_2 spectrum of fractured-type samples.

caused by the change of residual oil saturation in fractures during air flooding. Thus, pores with a pore radius greater than $11 \mu\text{m}$ are defined as fractures. It can be observed that air first enters the high-seepage fracture, and the T_2 spectrum signal at the fracture decreases, indicating that crude oil at the fracture is produced. With the increase of air injection volume, the air in the fracture gradually enters the core matrix, and the matrix crude oil is produced. When the injection volume is 0.6–0.8 PV, the envelope of the T_2 spectrum shifts to the left and decreases, and the oil in the small pores of the matrix decreases significantly, indicating that the crude oil in the core matrix migrates to the fracture, that is, the matrix supplies oil to the fracture. At this time, the mass transfer of crude oil at the core matrix and fracture can be attributed to the following three aspects. (1) The local LTO reaction occurs when the matrix crude oil comes in contact with the gas in the fracture, and the thermal effect causes the matrix crude to expand and decrease in viscosity. As a result, the generated thermal miscible flooding improves the fluidity of the oil, thereby improving matrix crude oil recovery. (2) Air migrates to the upper part of the core under the action of gravity differentiation and then sweeps the micropore crude oil in the matrix. Gas and crude oil can lead to LTO reaction through cross-flow, and the generated hydrocarbon compounds can

come in contact with the matrix “dead-end” pore crude oil. Thus, the interfacial tension of oil and gas decreases under mass exchange, which greatly reduces the seepage resistance of the matrix supplies oil to the fracture. (3) The CO_2 generated by the LTO reaction can be dissolved in matrix small-pore crude oil; hence, miscible or near-miscible flooding can occur in the narrow area near the shale matrix/fracture interface,^{26,45} and the matrix crude oil can be produced by extraction. In the later stage of air flooding, the recovery of crude oil in the matrix of the fractured-type sample is greatly improved; the fracture edge and the upper part of the matrix are the main residual oil enrichment areas.

Figure 15a presents the change of oil recovery under air flooding with different types of samples. The oil recovery in the matrix-type sample exhibits a trend of a slow and then a rapid increase, while the oil recovery in the fractured-type sample presents a trend of increasing rapidly and then slowly. The oil recoveries of the matrix-type sample and the fractured-type sample are 34.55 and 58.03%, respectively. When the air injection volume was 1.2 PV, the recoveries for small pores, medium pores, and macropores in the fractured-type sample reached 10.97, 19.89, and 27.17%, respectively; compared with the matrix-type sample, the recoveries of medium pores and macropores increased by 9.01 and 18.39%, respectively (Figure 15b). It can be concluded that the fracture can effectively improve the pore-throat connectivity of the reservoir and greatly improve oil recovery.

Figure 16 presents the residual oil saturation under air flooding with different types of samples. The residual oil saturation in the matrix-type sample reached 44.84, 19.65, and 0.96%, respectively. The residual oil saturation in the fractured-type sample reached 6.03, 32.88, and 3.06%, respectively. In general, at the same air injection volume, compared with the matrix-type sample air flooding, the residual oil saturation after the fractured-type sample air flooding is 23.49% lower, and especially in small pores, the residual oil saturation is 38.81% lower. The residual oil is mainly distributed in small pores and medium pores, which are the objects of further EOR.

The oil migration and seepage model of the fractured-type shale reservoir during air flooding is shown in Figure 17. The small pores in the matrix correspond to a larger capillary pressure and a stronger seepage resistance. Therefore, after shale

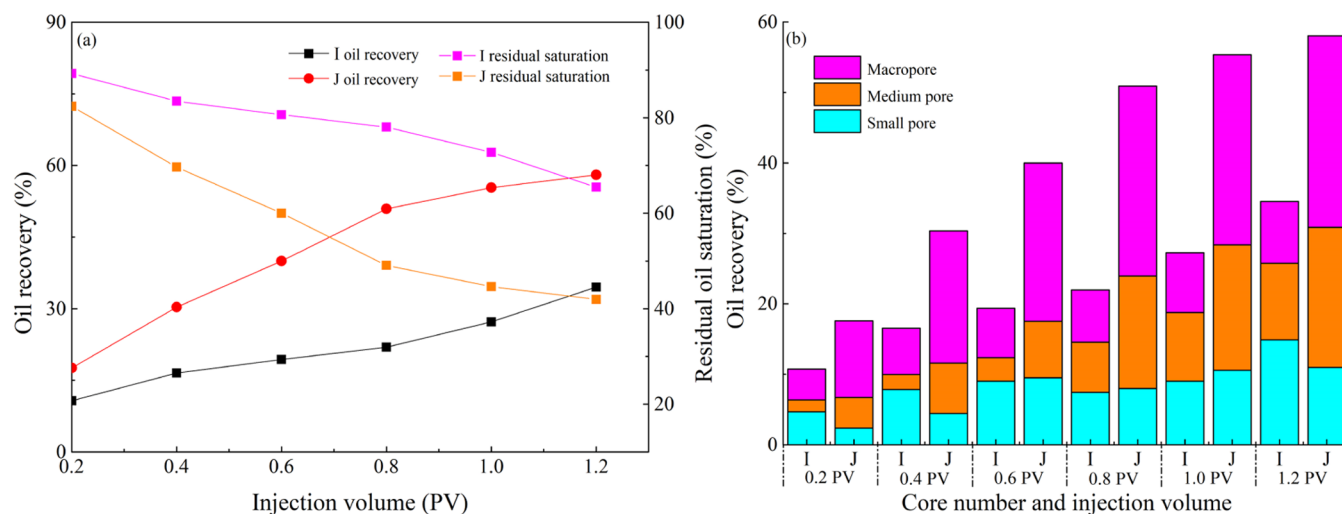


Figure 15. Change of total oil recovery (a) and different pore recoveries (b) with injection volume of air flooding with different types of samples.

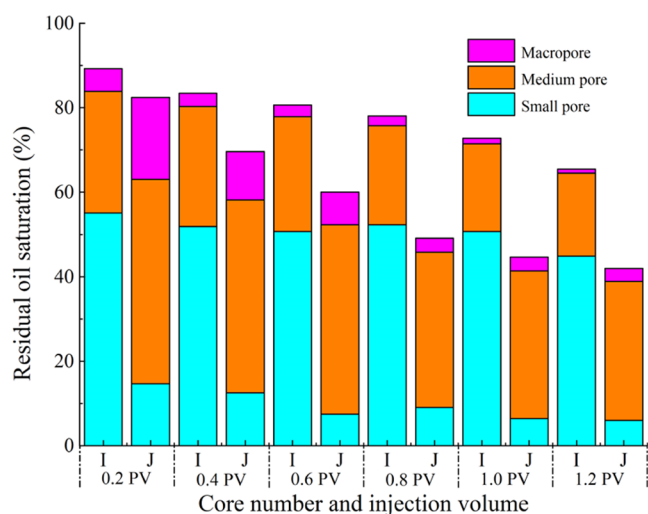


Figure 16. Change of residual oil saturation as a function of injection volume of air flooding with different types of samples.

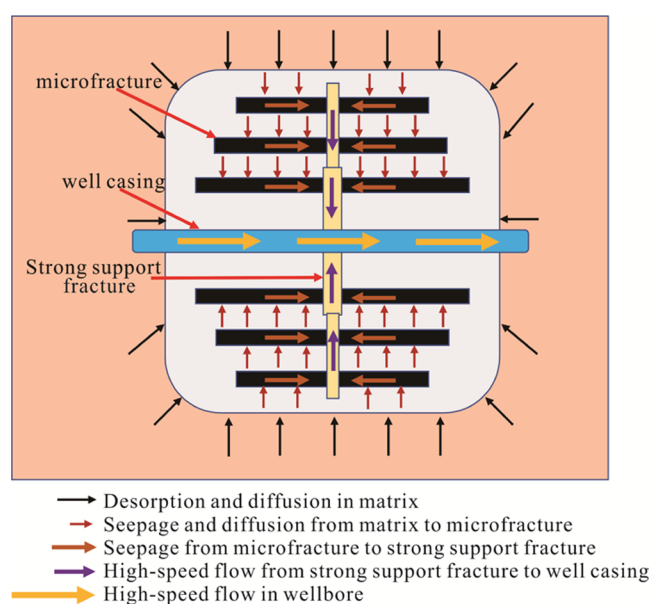


Figure 17. Oil migration and seepage model of the fractured-type shale reservoir during air flooding.

fracturing, the small-pore oil in the matrix tends to migrate to microfractures such as shale bedding fractures, while the oil collected in shale bedding fractures tends to migrate to strong support fractures; thus, microfractures such as bedding fractures can be regarded as bridges between the small pores of the matrix and the strong supporting fractures, which allows the crude oil to flow to the well casing and be produced.^{46,47} In fact, when fractures are developed in shale cores, crude oil in fractures and macropores can be discharged in the early stage of air flooding, and the pressure difference sweep plays a major role.³³ With the increase of air injection volume, the pressure will be transmitted to the small pores in the matrix, and the dissolution sweep will contribute more to the production of crude oil; hence, the recovery greatly increased. However, as the pore structure of the matrix-type sample deteriorates, the proportion of fractures decreases and less crude oil is deposited in larger pores; as a result, the total recovery is lower. It can be concluded that fractures can effectively increase the contact area between gas

and crude oil and the sweep range of the displacement front, decrease the seepage resistance and seepage distance during the migration of crude oil in the matrix, and improve the sweep efficiency and matrix drainage area.

5. CONCLUSIONS

In this study, the online NMR dynamic physical simulation experiment was conducted on air flooding in shale oil to overcome the pitfalls of using a conventional research method. This provides an effective way to intuitively quantify the recovery and residual oil saturation of crude oil with different pore sizes, and the microscopic production characteristics and displacement mechanism of shale oil by air flooding were analyzed. Additionally, the factors of shale oil by air flooding EOR were further discussed. The main conclusions of this study are as follows.

- (1) Shale oil is mainly distributed in three scales of pores in the range of 0.005–10 μm , and the proportion of small-pore crude oil gradually increases with the deterioration of permeability. The LTO reaction can occur by injecting air into depleted shale reservoirs, which has a certain effect on oil expansion, viscosity reduction, and thermal mixing phases, thereby greatly improving shale oil recovery, but there are significant differences in the production characteristics of different levels of pores.
- (2) The macropores have less flow resistance and are more conducive to gas flow compared with the small pores, and the production rate of the macropore oil was initially fast and then slow with a higher production degree. Meanwhile, the residual oil of air flooding in shale reservoirs is mainly distributed in medium pores and small pores less than 1 μm . There is a positive relationship between air oxygen concentration and oil recovery; the oxidation effect and viscosity reduction effect are more obvious at higher oxygen concentrations, which means that the oxygen concentration of air flooding can be increased within a safe range. High permeability means good pore-throat connectivity and greater oil recovery, and the production degree of crude oil in all pores increased significantly as the core permeability increased.
- (3) Appropriate injection pressure is beneficial to increasing the oil–gas contact time and delaying gas breakthrough, but high injection pressure will result in early gas channeling, which causes the crude oil in small pores to be difficult to produce. The recovery increases first and then decreases with the increase of injection pressure. Fractures can play a bridge role in the migration of matrix crude oil, reduce seepage resistance, increase the oil drainage area, and increase the production degree of matrix crude oil through mass exchange between matrix and fractures, which means that proper fracturing before gas injection can make the EOR better.

AUTHOR INFORMATION

Corresponding Authors

Meng Du – University of Chinese Academy of Sciences, Beijing 100049, China; Institute of Porous Flow & Fluid Mechanics, Chinese Academy of Sciences, Langfang 065007, China; Research Institute of Petroleum Exploration & Development, PetroChina, Beijing 100083, China; orcid.org/0009-0005-4587-4523; Email: dumeng22@mails.ucas.ac.cn

Zhengming Yang – University of Chinese Academy of Sciences, Beijing 100049, China; Research Institute of Petroleum Exploration & Development, PetroChina, Beijing 100083, China; Email: yzhm69@petrochina.com.cn

Authors

Chun Feng – Research Institute of Petroleum Exploration & Development, PetroChina, Beijing 100083, China

Lanlan Yao – University of Chinese Academy of Sciences, Beijing 100049, China; Research Institute of Petroleum Exploration & Development, PetroChina, Beijing 100083, China

Xinliang Chen – University of Chinese Academy of Sciences, Beijing 100049, China; State Key Laboratory of Enhanced Oil Recovery, Beijing 100083, China

Haibo Li – Research Institute of Petroleum Exploration & Development, PetroChina, Beijing 100083, China; State Key Laboratory of Enhanced Oil Recovery, Beijing 100083, China

Complete contact information is available at:

<https://pubs.acs.org/10.1021/acsomega.3c01585>

Notes

The authors declare no competing financial interest.

ACKNOWLEDGMENTS

This work was supported by the Major scientific and technological research projects of China Petroleum “Study on the Seepage Law of Typical Low-Grade Oil Reservoirs and New Methods for Enhancing Oil Recovery” (2021DJ1102) and the China Petroleum Science and Technology Major Project (2022kt1001).

REFERENCES

- (1) Li, Y.; Zhao, Q.; Lyu, Q.; Xue, Z.; Cao, X.; Liu, Z. Evaluation technology and practice of continental shale oil development in China. *Pet. Explor. Dev.* **2022**, *49*, 1098–1109.
- (2) Afagwu, C.; Alafnan, S.; Mahmoud, M.; Akkutlu, Y. Modeling of natural gas self-diffusion in the micro-pores of organic-rich shales coupling sorption and geomechanical effects. *J. Nat. Gas Sci. Eng.* **2022**, *106*, No. 104757.
- (3) Mukhina, E.; Cheremisin, A.; Khakimova, L.; Garipova, A.; Dvoretzskaya, E.; Zvada, M.; Kalacheva, D.; Prochukhan, K.; Kasyanenko, A.; Cheremisin, A. Enhanced oil recovery method selection for shale oil based on numerical simulations. *ACS Omega* **2021**, *6*, 23731–23741.
- (4) Jin, Z.; Zhu, R.; Liang, X.; Shen, Y. Several issues worthy of attention in current lacustrine shale oil exploration and development. *Pet. Explor. Dev.* **2021**, *48*, 1471–1484.
- (5) Aguilera, R. Flow units: from conventional to tight-gas to shale-gas to tight-oil to shale-oil reservoirs. *SPE Reservoir Eval. Eng.* **2014**, *17*, 190–208.
- (6) Lv, W.; Chen, S.; Gao, Y.; Kong, C.; Jia, N.; He, L.; Wang, R.; Li, J. Evaluating seepage radius of tight oil reservoir using digital core modeling approach. *J. Pet. Sci. Eng.* **2019**, *178*, 609–615.
- (7) Xue, C.; Ji, D.; Cheng, D.; Wen, Y.; Luo, H.; Li, Y.; et al. Adsorption behaviors of different components of shale oil in quartz slits studied by molecular simulation. *ACS Omega* **2022**, *7*, 41189–41200.
- (8) Javadpour, F.; Mclure, M.; Naraghi, M. E. Slip-corrected liquid permeability and its effect on hydraulic fracturing and fluid loss in shale. *Fuel* **2015**, *160*, 549–559.
- (9) Li, Y.; Di, Q.; Hua, S.; Jia, X.; et al. Visualization of foam migration characteristics and displacement mechanism in heterogeneous cores. *Colloids Surf., A* **2020**, *607*, No. 125336.
- (10) Yang, Z.; Li, R.; Li, H.; Luo, Y.; Chen, T.; Gao, T.; Zhang, Y. Experimental evaluation of the salt dissolution in inter-salt shale oil reservoirs. *Pet. Explor. Dev.* **2020**, *47*, 803–809.
- (11) Jiao, F. Re-recognition of “unconventional” in unconventional oil and gas. *Pet. Explor. Dev.* **2019**, *46*, 847–855.
- (12) Wang, J.; Ji, Z.; Liu, H.; Huang, Y.; Wang, Y.; Pu, Y. Experiments on nitrogen assisted gravity drainage in fractured-vuggy reservoirs. *Pet. Explor. Dev.* **2019**, *46*, 355–366.
- (13) Liao, G.; Yang, H.; Jiang, Y.; Ren, S.; Li, D.; Wang, L.; Wang, Z.; Wang, B.; Liu, W. Applicable scope of oxygen-reduced air flooding and the limit of oxygen content. *Pet. Explor. Dev.* **2018**, *45*, 111–117.
- (14) Al-shargabi, M.; Davoodi, S.; Wood, D.; Rukavishnikov, V.; Minaev, K. Carbon Dioxide applications for enhanced oil recovery assisted by nanoparticles: recent developments. *ACS Omega* **2022**, *7*, 9984–9994.
- (15) Qian, C.; Luo, F.; Jiang, Z.; Qi, L.; Feng, L. EOR experiment of air injection displacement and low-temperature oxidation reaction characteristics in low-permeability reservoirs. *Pet. Geol. Oilfield Dev. Daqing* **2022**, *41*, 97–103.
- (16) Kok, M. V.; Gul, K. G. Thermal characteristics and kinetics of crude oils and SARA fractions. *Thermochim. Acta* **2013**, *569*, 66–70.
- (17) Liao, G.; Wang, H.; Wang, Z.; Tang, J.; Wang, B.; Pan, J.; Yang, H.; Liu, W.; Song, Q.; Pu, W. Oil oxidation in the whole temperature regions during oil reservoir air injection and development methods. *Pet. Explor. Dev.* **2020**, *47*, 357–364.
- (18) Ren, S. R.; Greaves, M.; Rathbone, R. Air injection LTO process: An IOR technique for light-oil reservoirs. *SPE J.* **2002**, *7*, 90–99.
- (19) Wang, J.; Wang, T.; Feng, C.; Yang, C.; Chen, Z.; Lu, G. Catalytic Effect of Transition Metallic Additives on the Light Oil Low Temperature Oxidation Reaction. *Energy Fuels* **2015**, *29*, 3545–3555.
- (20) Hou, S.; Liu, Y.; Yu, H.; Niu, B.; Ren, S. R. Kinetics of low temperature oxidation of light oil in air injection process. *J. China Univ. Pet. (Nat. Sci. Ed.)* **2011**, *35*, 169–173.
- (21) Long, A.; Zhang, M.; Song, H. Study on mechanism of low temperature oxidation reaction of deoxidized air drive: Taking E3 1 reservoir of Gaskule oilfield as an example. *China Energy Environ. Prot.* **2020**, *42*, 105–109.
- (22) Mothé, C. G.; De Miranda, I. C. Study of kinetic parameters of thermal decomposition of bagasse and sugarcane straw using Friedman and Ozawa-Flynn-Wall iso conversional methods. *J. Therm. Anal. Calorim.* **2013**, *113*, 497–505.
- (23) Zhang, Y.; Huang, S.; Sheng, J.; Jiang, Q. Experimental and analytical study of oxygen consumption during air injection in shale oil reservoirs. *Fuel* **2020**, *262*, No. 116462.
- (24) Youwei, J.; Zhang, Y.; Liu, S.; Guan, W.; Chen, Y.; Liu, S. Displacement mechanisms of air injection in low permeability reservoirs. *Pet. Explor. Dev.* **2010**, *37*, 471–476.
- (25) Chen, X.; Li, Y.; Liao, G.; Zhang, C.; Xu, S.; Qi, H.; Tang, X. Experimental investigation on stable displacement mechanism and oil recovery enhancement of oxygen-reduced air assisted gravity drainage. *Pet. Explor. Dev.* **2020**, *47*, 836–845.
- (26) Qi, H.; Li, Y.; Chen, X.; Long, A.; Wei, L.; Li, J.; Luo, J.; Sun, X.; Tang, X.; Guan, C. Low-temperature oxidation of light crude oil in oxygen-reduced air flooding. *Pet. Explor. Dev.* **2021**, *48*, 1393–1402.
- (27) Li, L.; Su, Y.; Hao, Y.; Zhan, S.; Lv, Y.; et al. A comparative study of CO₂ and N₂ huff-n-puff EOR performance in shale oil production. *J. Pet. Sci. Eng.* **2019**, *181*, No. 106174.
- (28) Yu, H.; Xu, H.; Fu, W.; Lu, X.; Chen, Z.; Qi, S.; Wang, Y.; Yang, W.; Lu, J. Extraction of shale oil with supercritical CO₂: Effects of number of fractures and injection pressure. *Fuel* **2021**, *285*, No. 118977.
- (29) Nguyen, P.; Willam, C.; Viswanathan, H.; Mark, P. Effectiveness of supercritical-CO₂ and N₂ huff-and-puff methods of enhanced oil recovery in shale fracture networks using microfluidic experiments. *Appl. Energy* **2018**, *230*, 160–174.
- (30) Al-Mudhafar, W. J. Polynomial and nonparametric regressions for efficient predictive proxy metamodeling: Application through the CO₂-EOR in shale oil reservoirs. *J. Nat. Gas Sci. Eng.* **2019**, *72*, No. 103038.
- (31) Burrows, L. C.; Haeri, F.; Cvetic, P.; Sanguinito, S.; Shi, F.; Tapriyal, D.; Goodman, A.; Enick, R. M. A Literature Review of CO₂, Natural Gas, and Water-Based Fluids for Enhanced Oil Recovery in Unconventional Reservoirs. *Energy Fuels* **2020**, *34*, 5331–5380.

- (32) Zhang, W.; Feng, Q.; Wang, S.; Xing, X.; Jin, Z. CO₂-regulated octane flow in calcite nanopores from molecular perspectives. *Fuel* **2021**, *286*, No. 119299.
- (33) Wan, T.; Zhang, J.; Jing, Z. Experimental evaluation of enhanced shale oil recovery in pore scale by CO₂ in Jimusar reservoir. *J. Pet. Sci. Eng.* **2022**, *208*, No. 109730.
- (34) Huang, X.; Li, X.; Zhang, Y.; Li, T.; Zhang, R. Microscopic production characteristics of crude oil in nanopores of shale oil reservoirs during CO₂ huff and puff. *Pet. Explor. Dev.* **2022**, *49*, 636–643.
- (35) Zhu, C.; Sheng, J.; Etehadtavakkol, A.; Li, Y.; Gong, H.; Li, Z.; Dong, M. Numerical and Experimental Study of Enhanced Shale-Oil Recovery by CO₂ Miscible Displacement with NMR. *Energy Fuels* **2020**, *34*, 1524–1536.
- (36) Dai, C.; Cheng, R.; Sun, X.; Liu, Y.; Zhou, H.; Wu, Y.; You, Q.; Zhang, Y.; Sun, Y. Oil migration in nanometer to micrometer sized pores of tight oil sandstone during dynamic surfactant imbibition with online NMR. *Fuel* **2019**, *245*, 544–553.
- (37) Wang, C.; Gao, H.; Qi, Y.; et al. Investigation on the mechanisms of spontaneous imbibition at high pressures for tight oil recovery. *ACS Omega* **2020**, *5*, 12727–12734.
- (38) Zhang, W.; Feng, Q.; Wang, S.; Xing, X.; Jin, Z. CO₂-regulated octane flow in calcite nanopores from molecular perspectives. *Fuel* **2021**, *286*, No. 119299.
- (39) Luo, Y.; Zhen, T.; Xiao, H.; Liu, X.; Zhang, H.; Wu, Z.; Zhao, X.; Xia, D.; et al. Identification of distinctions of immiscible CO₂ huff and puff performance in Chang-7 tight sandstone oil reservoir by applying NMR, microscope and reservoir simulation. *J. Pet. Sci. Eng.* **2022**, *209*, No. 109719.
- (40) Gutierrez, D.; Skoreyko, F.; Moore, R.; Mehta, S.; Ursenbach, M. The challenge of predicting field performance of air injection projects based on laboratory and numerical modelling. *J. Can. Pet. Technol.* **2009**, *48*, 23–33.
- (41) Xi, C.; Wang, B.; Zhao, F.; Liu, T.; Qi, Z.; Zhang, X.; Tang, J.; Jiang, Y.; Guan, W.; Wang, H.; et al. Oxidization characteristics and thermal miscible flooding of high-pressure air injection in light oil reservoirs. *Pet. Explor. Dev.* **2022**, *49*, 874–884.
- (42) Zhong, X.; Zhu, Y.; Liu, L.; Yang, H.; Li, Y.; Xie, Y.; Liu, L. The characteristics and influencing factors of permeability stress sensitivity of tight sandstone reservoirs. *J. Pet. Sci. Eng.* **2020**, *191*, No. 107221.
- (43) Al-Mudhafar, W. J. From core flooding and scaled physical model experiments to field-scale enhanced oil recovery evaluations: Comprehensive review of the gas-assisted gravity drainage process. *Energy Fuels* **2018**, *32*, 11067–11079.
- (44) Du, M.; Xiang, Y.; Jia, N.; Lv, W.; Zhang, J.; Zhang, D. Pore structure characteristics of tight glutenite reservoir of Baikouquan Formation in Mahu Sag. *Lithol. Reserv.* **2021**, *33*, 120–131.
- (45) Lang, D.; Lun, Z.; Lyu, C.; Wang, H.; Zhao, Q.; Sheng, H. Nuclear magnetic resonance experimental study of CO₂ injection to enhance shale oil recovery. *Pet. Explor. Dev.* **2021**, *48*, 702–712.
- (46) Bai, M.; Zhang, Z.; Chen, Q.; Shao, W.; Du, S. Research on the enhanced oil recovery technique of horizontal well volume fracturing and CO₂ huff-n-puff in tight oil reservoirs. *ACS Omega* **2021**, *6*, 28485–28495.
- (47) Forstner, S. R.; Laubach, S. Scale-dependent fracture networks. *J. Struct. Geol.* **2022**, *165*, No. 104748.